

Article

Growth and Characterization of Organic 2-Chloro 5-Nitroaniline Crystal Using the Vertical Bridgman Technique

Shanmugam Karuppusamy^{1,2}, Veerappampalayam Easwaramoorthy Sathishkumar³, Kanagaraj Dinesh Babu⁴ and Pandurengan Sakthivel^{5,*} 

¹ Department of Physics, Anna University, Chennai 600025, India; ssksamy@gmail.com

² Department of Physics, Excel Engineering College, Komarapalaym 637303, India

³ Department of Software Engineering, Jeonbuk National University, Jeonju-si 54896, Jeollabuk-do, Republic of Korea; sathish@jbnu.ac.kr

⁴ Department of Electrical and Electronics Engineering, Sri Shakthi Institute of Engineering and Technology, Coimbatore 641062, India; dineshbabu102@gmail.com

⁵ Centre for Materials Science, Science and Humanities, Faculty of Engineering, Karpagam Academy of Higher Education, Coimbatore 641021, India

* Correspondence: sakthi1807@gmail.com

Abstract: In this article, we discuss the preparation of organic 2-chloro-5 nitroaniline (2C5NA) crystals and their different kinds of physical, chemical, and mechanical properties. The vertical Bridgman approach was used to effectively produce the bulk organic 2C5NA crystal. To produce a good-quality bulk crystal, the shape, dimensions, and cone angle of the ampoule were optimized. Also, the temperature profile was set for the 2C5NA crystal. The growth atmosphere and the lowering rate were identified to obtain a homogeneous mixture of the compounds and initiate the nucleation process. Single-crystal X-ray diffraction (XRD), powder XRD, proton Fourier transform nuclear magnetic resonance (FT-NMR), and Fourier transform infrared investigations were used to confirm the crystal structure, molecular structure, and presence of functional groups in the formed crystal. The formed crystal has a monoclinic crystal structure with the space group P21/c, according to single-crystal XRD analysis. The thermal stability and kinetic parameters were examined using thermogravimetric analysis and differential thermal curves. From dielectric analysis, the electrical conductivity and dielectric behavior of 2C5NA were investigated with variations in frequency and temperature. The organic 2-chloro-5-nitroaniline crystal demonstrates that the indentation size effect is observed in the Vickers micro-hardness test, which was also carried out.

Keywords: 4-nitrophenol crystal; vertical Bridgman technique; thermal kinetics; dielectric behavior; mechanical behavior



Citation: Karuppusamy, S.; Sathishkumar, V.E.; Dinesh Babu, K.; Sakthivel, P. Growth and Characterization of Organic 2-Chloro 5-Nitroaniline Crystal Using the Vertical Bridgman Technique. *Crystals* **2023**, *13*, 1349. <https://doi.org/10.3390/cryst13091349>

Academic Editors: Xiping Zhang and Alexander Y. Nazarenko

Received: 15 July 2023

Revised: 30 August 2023

Accepted: 1 September 2023

Published: 5 September 2023



Copyright: © 2023 by the authors. Licensee MDPI, Basel, Switzerland. This article is an open access article distributed under the terms and conditions of the Creative Commons Attribution (CC BY) license (<https://creativecommons.org/licenses/by/4.0/>).

1. Introduction

2-Chloro-5-nitroaniline (2C5NA) is a simple organic compound that has an electron-donating NH₂ group and an electron-acceptor NO₂ group at the fifth position. It is also chlorine attached at the second position of the aromatic ring [1]. It finds applications in the field of organic chemistry and can be used as an intermediate in the synthesis of various pharmaceuticals, dyes, and agrochemicals. It can also be employed as a starting material in the production of other compounds with specific chemical properties. Substituted aniline and nitrobenzene derivative compounds are valuable intermediators for a variety of pigments, dyes, rubber chemicals, etc. [2,3]. For coupling and developing color films, the 2C5NA compound is used as an intermediator. The interactions of intermolecular molecules and the structure of the crystals influence the physical and chemical properties of the crystal. Moreover, the reaction schemes can also be tuned to acquire nonlinear behavior. Centrosymmetric crystals, also known as inversion-symmetric crystals, are a type of crystal structure that possesses a center of symmetry. Centrosymmetric crystals are quite common

and include various mineral crystals, such as quartz, calcite, and fluorite. They are also found in many synthetic crystals and materials used in various technological applications. Generally, centrosymmetric crystals do not exhibit second harmonic generation efficiency (SHG); however, they give rise to third-order nonlinear behavior [4,5]. Third harmonic generation (THG) is a nonlinear optical process in which three photons with the same frequency interact within a material, resulting in the generation of a new photon with triple the frequency (three times the energy) of the incident photons. THG is a type of frequency-tripling process. The major applications of third harmonic generation (THG) are optical signal processing, photonic waveguides [6], frequency-resolving optical gating, and optical imaging processing [7]. The investigation of chlorinated benzene compounds is a difficult process due to their toxicity. Though they are toxic compounds, their thermal and kinetic properties should be well-understood in order to avoid unwanted chemical reactivity with the environment during the decomposition process. For the title compound, the formation of enthalpy at various states, such as crystalline solids, liquids, and gases, was obtained and compared with theoretically evaluated values [8].

Two nitrobenzoic acids, some halogenated nitroanilines, and nine novel 1:1 co-crystals of caffeine have been created. They exhibit brittle fractures when a mechanical load is applied [9]. The salts of 2-chloro-4-nitroaniline and 2-methyl-6-nitroaniline were reanalyzed structurally and theoretically. According to theoretical calculations of the relaxed potential energy surface (rPES), the energy barriers for the rotation of the nitro group in isolated $\text{H}_2\text{Cl}_4\text{Na}^+$ and $\text{H}_2\text{m}_6\text{Na}^+$ cations are 4.6 and 11.6 kcal mol⁻¹, respectively [10]. The dispersion of organic N-benzyl-2-methyl-4-nitroaniline (BNA) in nematic liquid crystals (LCs) was studied. BNA doping decreases the cell's threshold voltage because the LC mixture has a higher dielectric anisotropy and a lower splay elastic constant. Due to decreases in the cell's threshold voltage and the rotational viscosity of the LC mixture, BNA-doped LC cells fall five times faster than pure ones when used in high voltage-differential scenarios. The BNA's spontaneous polarization electric field (SPEF), which induces an extra restoring force, helps to shorten LC cells' fall time [11].

A series of new anthranilic diamide analogues (12a–12u) comprising N-substituted phenylpyrazole were designed and synthesized in order to find effective insecticides that target ryanodine receptors (RyRs). These chemicals showed moderate to exceptional insecticidal effects, according to their insecticidal activities. In particular, 12i demonstrated 100 and 37% larvicidal effects at 0.25 and 0.05 mg L⁻¹ against oriental armyworm (*Mythimna separata*), which are equal to those of chlorantraniliprole (100%, 0.25 mg L⁻¹; and 33%, 0.05 mg L⁻¹) [12]. The molecular complex of 2-methyl-4-nitroaniline and trichloroacetic acid, also known as 2-methyl-4-nitroanilinium trichloroacetate trichloroacetic acid ($\text{C}_{11}\text{H}_{10}\text{Cl}_3\text{N}_2\text{O}_6$), has been the subject of structural studies using single-crystal and powder X-ray diffraction methods [13]. Based on information from the X-ray co-crystal structure of BRAE, the novel tertiary 1-cyano-1-methylethoxy substituent was created to occupy the hydrophobic region of the protein's "back pocket". We also discovered that the amine linker's N-methylation might influence the twisted molecular shape, improving solubility [14]. By using single-crystal X-ray diffraction, the crystal structures of three novel salts of 2-methyl-3-nitroaniline with inorganic acids— $(\text{H}_2\text{m}_3\text{Na})\text{NO}_3$, $(\text{H}_2\text{m}_3\text{Na})_2\text{SO}_4$, and $(\text{H}_2\text{m}_3\text{Na})\text{H}_2\text{PO}_4$ —were identified. The nitro group is not plane with respect to the benzene ring for the structure of the global minimum, which is an unusual conformation among nitroanilines, according to theoretical calculations of the relaxed potential surface [15]. Analyzing the solidification behavior of organic molecules is a very complex process, as they undergo several natural variations in their thermal stability. Hence, only a few organic materials satisfied the melt growth conditions and were adopted to grow into crystals using the melt growth technique. In the case of the title compound, there was no weight loss observed before its melting point, so we adopted the melt growth technique to grow the bulk crystal. The crystal growth of 2C5NA, via the vertical Bridgman technique using a single-wall ampoule, and its characterization are discussed in this paper. In this method, by controlling the temperature gradient and the pulling rate of the crucible, the quality and

properties of the crystal can be optimized. The vertical Bridgman technique offers several advantages in crystal growth, including the ability to control crystal composition and doping, as well as a relatively simple setup and operation. However, it also has limitations, such as the possibility of introducing dislocations and defects during the growth process. The cone angle of the ampoule and the physico-chemical, dielectrical, and mechanical properties of 2C5NA crystal, which were examined using various characterization techniques such as single-crystal XRD, powder XRD, proton NMR, FTIR, thermal analysis, dielectric studies, and Vicker's microhardness test, are elaborated on in detail. Using the Kissinger and Ozawa methods, thermal kinetic parameters were estimated, and from an Arrhenius plot, the thermal and electrical activation energies of the 2C5NA compound were evaluated.

2. Materials and Methods

Through numerous recrystallization procedures, the 2C5NA chemical, which is commercially accessible, was purified. The chemical structure of 2C5NA is represented in Figure 1. Methanol was used as a solvent and 200 mL of supersaturated solution was prepared in a beaker that was kept at room temperature for the recrystallization process. The solution evaporates fast at room temperature; hence, the beaker was tightly covered with polythene paper. Several single and polycrystalline crystals were obtained from the solution growth technique over the course of a week. Good-quality crystals were chosen from the beaker and ground into a fine powder. The powdered feed sample was loaded into a thoroughly washed borosilicate glass ampoule. The density of the title compound is low; hence, the large volume of the ampoule is occupied. The dimensions and cone angles of the ampoule are illustrated in Figure 2. The quality of the crystal can be evaluated using the results obtained from P-XRD, HR-XRD, TG-DTA curve, and cone angle. The cone angle plays a vital role in initiating the nucleation process. The decomposition and melting points are very close for organic molecules. This property can affect the crystalline nature; if we use a very low cone angle, we can avoid the decomposition process before the crystallization process. The cone angle was optimized to be $13^{\circ}40'$ for the 2C5NA growth ampoule. Generally, ampoules with cone angles between 10 and 20° are preferred to obtain good-quality crystals without twinning and strain due to ampoule walls.

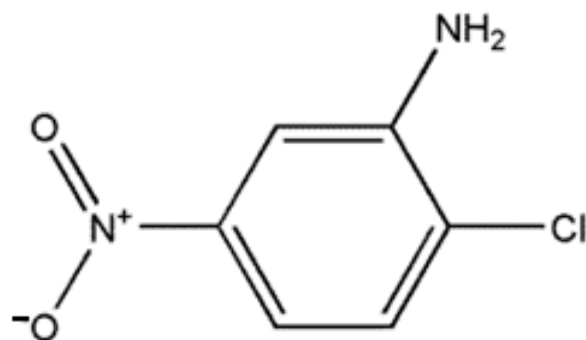


Figure 1. The chemical structure of 2C5NA.

Owing to the fast translation of the ampoule, the cleavage planes and multiplication of nucleation were formed. The 2C5NA compound was decomposed when the experiment was carried out at a low translation rate (below 0.5 mm/h). It may have occurred due to the formation of reactions with the outer atmosphere, melt inhomogeneity, and poor thermal stability beyond their melting point. Depending on the melting temperature of the title compound, the temperature profile of the furnace was optimized (Figure 3).

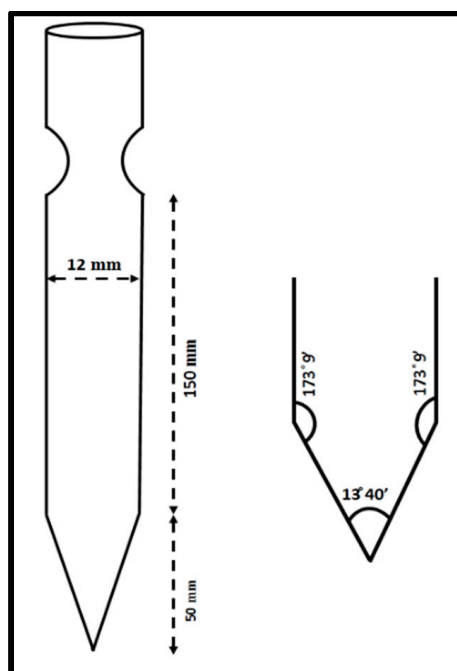


Figure 2. Schematic diagram of the ampoule and its cone angle.

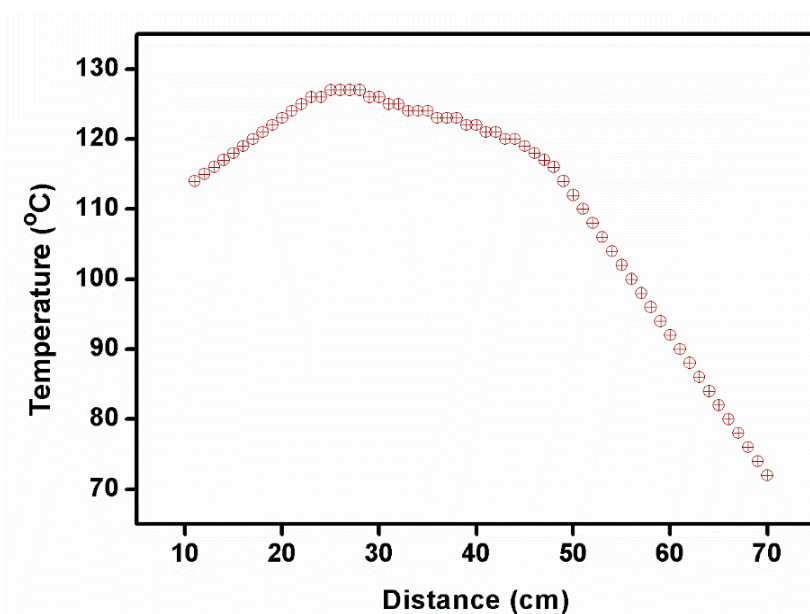


Figure 3. Temperature profile of furnace used to grow the 2C5NA crystal.

The lowering rate of the ampoule was maintained at approximately 0.7–0.8 mm/h. As discussed in previous chapters, when lowering the ampoule at an optimized lowering rate, the powder melts at its melting temperature, and nucleation is initiated at its crystallization temperature. Due to the large volume of sample loaded into the ampoule (Figure 4a), the bottom portion of the ampoule was completely melted, while the top portion of the ampoule was partially melted. The homogeneity and uniformity of the bulk crystal were affected by the uneven melting of the sample. Hence, several trials were attempted to achieve a homogeneous 2C5NA crystal. The grown crystal of 2C5NA is shown in Figure 4b.

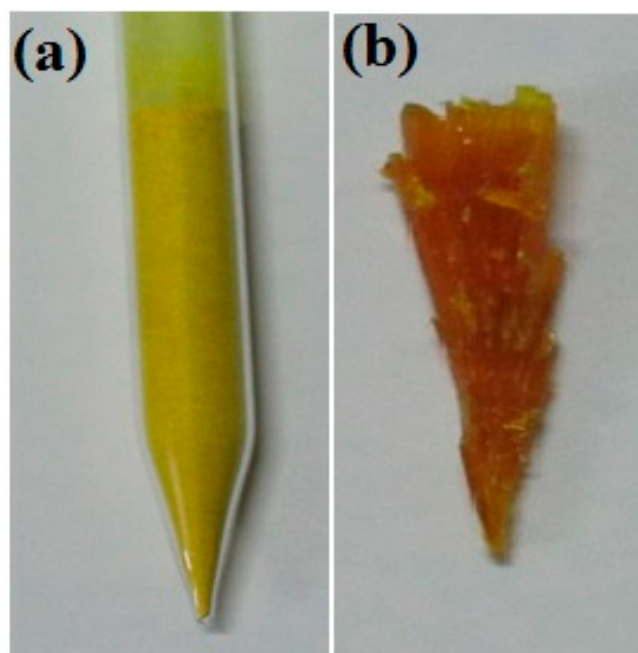


Figure 4. (a) Loaded ampoule. (b) Grown crystal of 2C5NA.

The lattice parameters and space group of the aforementioned compound were examined at room temperature using a Bruker AXS Kappa APEX-II single-crystal X-ray diffractometer (Bruker, Billerica, MA, USA). Additionally, powder XRD tests were performed using a Bruker D2 PHASER apparatus. CuK α radiation (1.5406 Å) was used for measurements in the 10–70° range with a scanning rate of 0.02°/S. The chemical composition of the 2C5NA crystal was confirmed by 1H. Deuterated methanol was used as the solvent to obtain NMR spectra (BRUKER, Billerica, MA, USA) using a BRUKER ADVANCE-III 500 MHz spectrometer. The FTIR spectrum (BRUKER, Billerica, MA, USA) of 2C5NA was recorded using Bruker ALPHA in KBr pellet mode between 500 and 4000 cm⁻¹. The thermal stability of 2A4MPPP (HITACHI, Tokyo, Japan) was tested between room temperature and 400 °C using a HITACHI-STA-7300. At varied heating rates, TG-DTA discovered thermal kinetic parameters. A silver-coated <010> orientated 2C5NA crystal with the dimensions of 8.09 × 5.63 × 1.87 mm³ was used as the dielectric in a parallel plate capacitor, and measurements of the dielectric were made using an HIOKI 3532-50 LCR HITESTER (KIOKI, Nagoya, Japan). The capacitance values were recorded at different temperatures, such as 40, 50, 60, 70, and 80 °C, while the applied frequency ranged from 50 Hz to 5 MHz. The mechanical hardness was assessed using MATSUZAWA MMT-X equipment (MATSUZAWA, Toshima, Japan). Vicker's hardness tester (MATSUZAWA, Toshima, Japan) was used to test the crystal's hardness while it was at room temperature and with applied loads ranging from 1 to 100 g.

3. Results and Discussion

3.1. X-ray Diffraction Analysis of 2C5NA

Single-crystal X-ray diffraction is a powerful technique used to determine the atomic structure of crystalline materials. It is particularly useful for studying single crystals, which are solid materials, composed of a regular repeating pattern of atoms. It allows for the determination of the precise atomic arrangement of crystals, providing valuable information about the crystal's chemical composition, bond lengths, different crystal phases, and polymorphs of a material. It can provide insight into crystal defects, disorder, and other structural imperfections. The centrosymmetric space group of P21/n in the monoclinic crystal structure of the prepared single crystal of 2C5NA was confirmed with single-crystal XRD. The lattice parameter values and volume were obtained as follows: $a = 13.66$ (18) Å, $b = 3.78$ (6) Å, $c = 13.67$ (20) Å, $\beta = 91.68$ (6)°, and volume $V = 706$ (3) Å³. The powder XRD

pattern of the 2C5NA with the peak indexations is depicted in Figure 5. High-intensity peaks of the powder XRD pattern were indexed using powder-X software (XBROAD, Crystal Growth Centre, Anna University, Chennai). The unit cell parameter values of single-crystal XRD data are closely matched with the reported values [16].

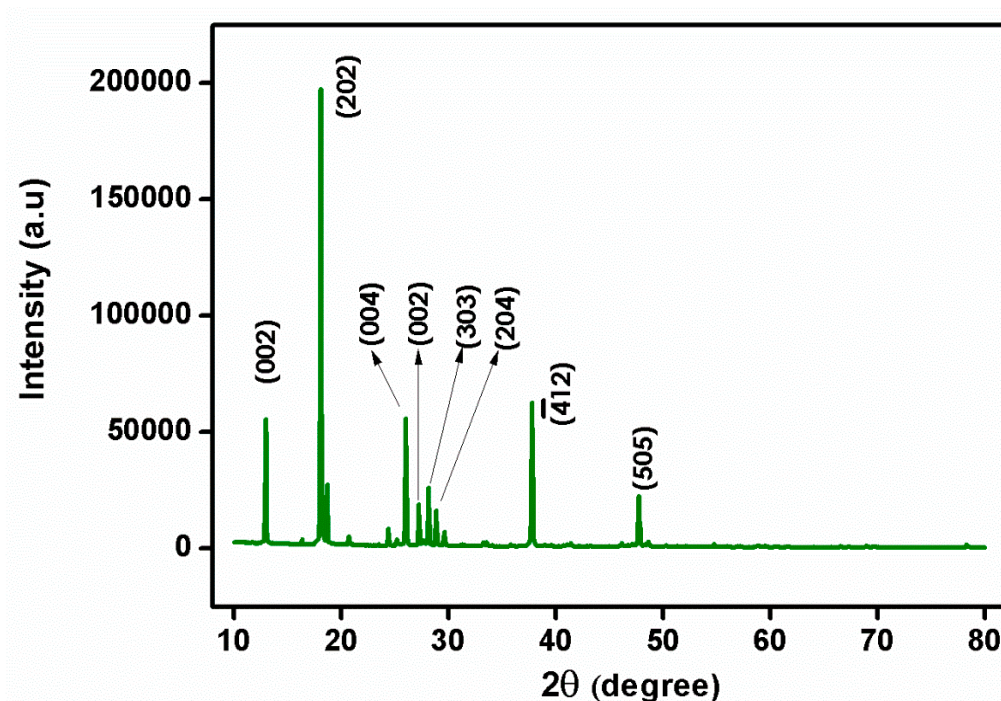


Figure 5. Powder XRD pattern of 2C5NA.

3.2. Proton NMR Spectral Analysis of 2C5NA

Proton nuclear magnetic resonance (NMR) spectral analysis is a powerful analytical technique used to study the molecular structure and environment of hydrogen atoms (protons) in organic and inorganic compounds. It is a non-destructive method based on the principle of nuclear magnetic resonance, where atomic nuclei with an odd number of protons or neutrons behave like tiny magnets in an external magnetic field. To establish the molecular structure of 2C5NA, the proton NMR spectrum (Figure 6) was recorded with deuterated methanol as the solvent. The chemical shifts in the spectrum revealed the structure of the 2C5NA crystal. The singlet peak observed at 4.42 ppm is attributed to the presence of the NH_2 group. Then, other multiplet signals (7.27, 7.39, 7.52, and 7.61 ppm) are ascribed to the CH bonds of different environments [17,18]. The C-13 NMR spectrum (Figure 7) was taken with deuterated methanol as a solvent to confirm the molecular structure of 2C5NA. The peaks appearing at 147.5, 143.68, 129.92, and 125.26 ppm are due to C-in aromatic rings and C=C (in alkenes). The peaks noticed near 113.28 and 109.72 ppm are indexed to nitriles ($\text{R}_\text{C}=\text{N}$). The multi-peaks observed around 77.37, 77.04 and 76.73 ppm are endorsed by alkyne C=C-H. The molecular structure of the 2C5NA crystal was validated and it shows a slight change in the chemical environment, which modifies the chemical shift.

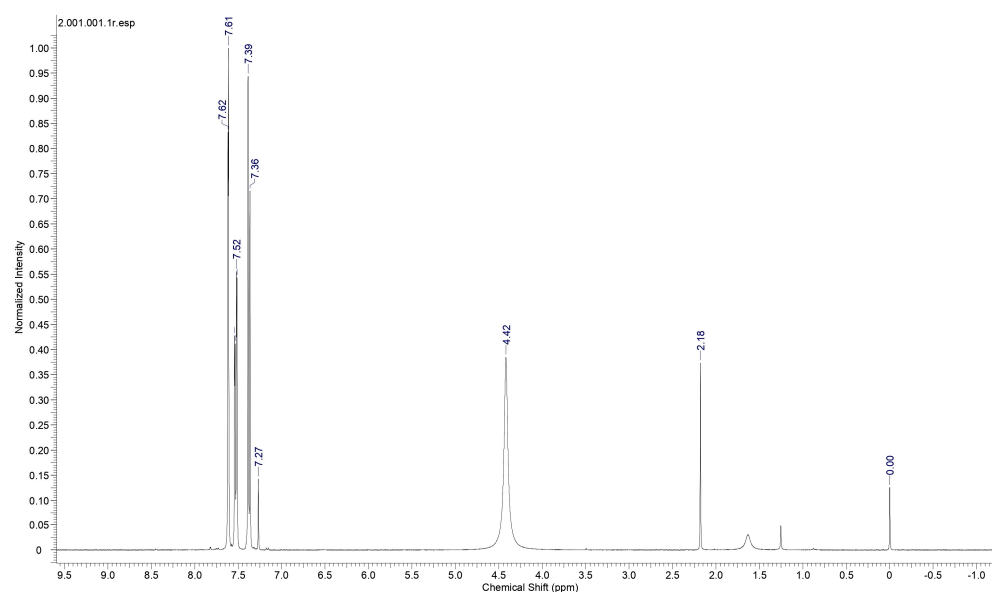


Figure 6. Proton ^1H NMR spectrum of 2C5NA.

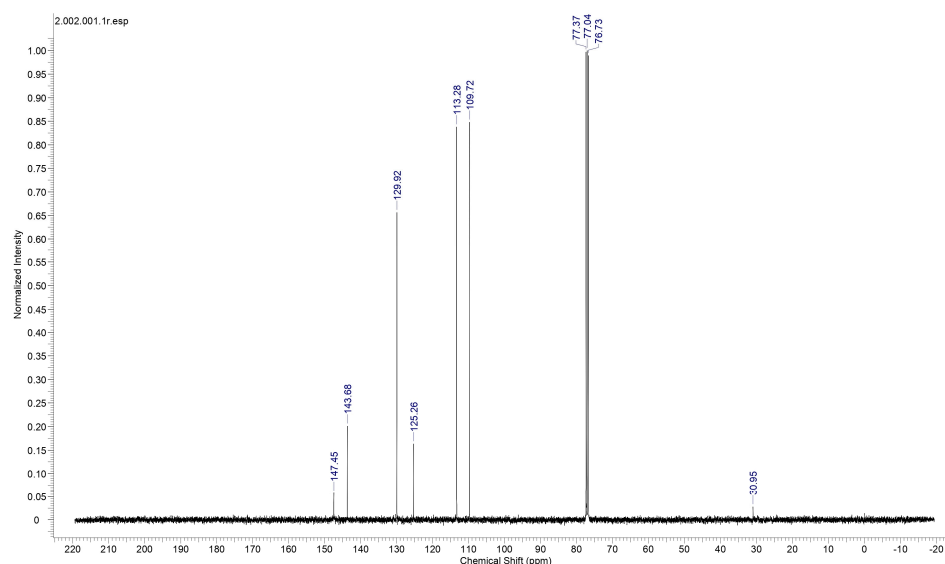


Figure 7. Proton ^{13}C NMR spectrum of 2C5NA.

3.3. FTIR Spectral Analysis of 2C5NA

FTIR spectral analysis is a widely used analytical technique for identifying and characterizing the chemical composition of a wide range of materials. It is based on the principle that molecules absorb infrared radiation at specific frequencies, which are related to the vibrational motions of the atoms in the molecule. Infrared spectra have become a potential tool to obtain information about functional groups in organic molecules when they are irradiated with a particular frequency. It can reveal important structural features of complex organic molecules [19]. FTIR spectroscopy, in particular, is a non-destructive, cost-effective tool for determining the functional group of any organic compound. The FTIR spectrum of 2C5NA is illustrated in Figure 8. The strong peak that appears at 736 cm^{-1} is assigned to the C-Cl stretching vibration. Aromatic C-H out-plane vibrations are observed in the region of $1000\text{--}700\text{ cm}^{-1}$. The C-N stretching vibration peak exists at 1042 cm^{-1} . The peaks at 1507 and 1347 cm^{-1} are bending vibrations of the NO_2 group. The N-H stretching peak (primary amine) is observed at 1625 , 3319 , and 3431 cm^{-1} and the position of the functional group depends on the degree of hydrogen bonds. The peaks at 1625 , 3319 , and

3431 cm^{-1} are ascribed to the presence of N-H (primary amine) bending vibrations. The C-H stretching vibrations of the benzene ring are observed at 3099 cm^{-1} [20].

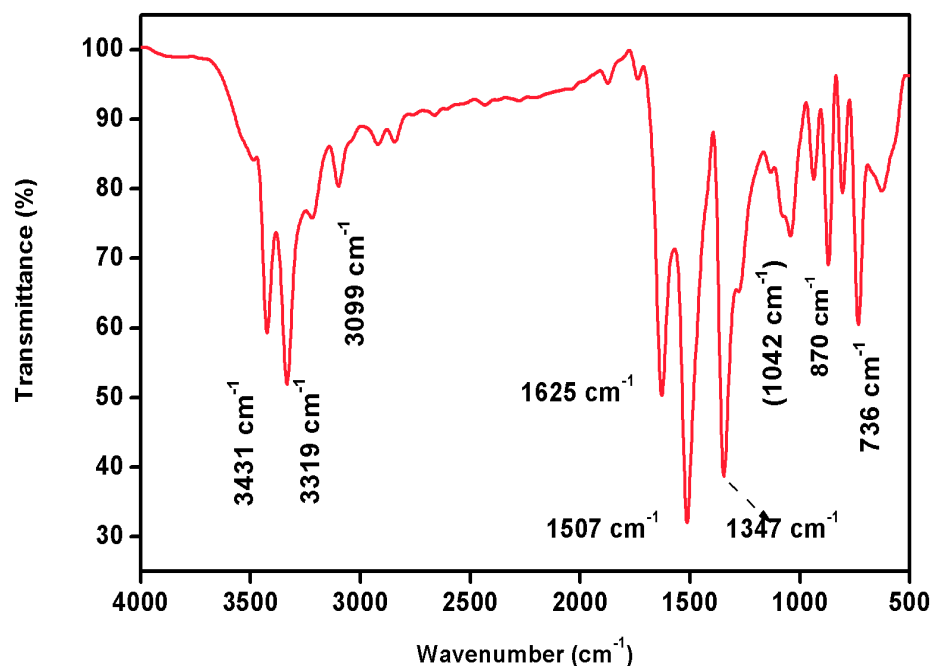


Figure 8. FTIR spectrum of 2C5NA.

3.4. Thermal Analysis of 2C5NA

Thermal analysis of crystals is a set of techniques used to study the physical and chemical properties of crystalline materials as they are subjected to changes in temperature. These methods are valuable for understanding phase transitions, thermal stability, thermal decomposition, and other thermal behaviors of crystals. Two common thermal analysis techniques are differential scanning calorimetry (DSC) and thermogravimetric analysis (TGA). The thermal behavior of 2C5NA was analyzed using a TG-DTA thermal analyzer. The thermogram of TG-DTA is depicted in Figure 9.

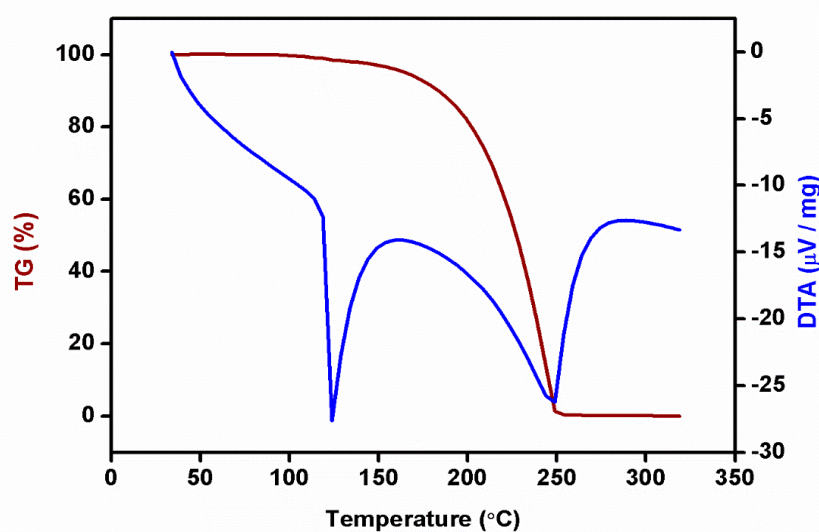


Figure 9. TG-DTA curve of 2C5NA.

The compound showed good thermal stability up to $110\text{ }^{\circ}\text{C}$, beyond which it started to melt. In the DTA curve, two sharp endothermic peaks were observed at 122 and $245\text{ }^{\circ}\text{C}$, which correspond to the melting and decomposition temperatures of the title material,

respectively. The TG curve exposed the weight loss of the sample around 150 °C and it continued until complete decomposition of the sample, which occurred at 245 °C. The complete weight loss of the TG curve also coincided with the second endothermic peak of the DTA curve. The thermal kinetic parameters for the melting temperature of 2C5NA were calculated using the Kissinger and Ozawa methods.

$$\ln \left[\frac{\beta}{T_m^2} \right] = \frac{-E_a}{RT_m} + \ln \left[\frac{K_0 R}{E_a} \right] \quad (1)$$

$$\ln(\beta) = \frac{-E_a}{RT_m} + \ln \left[\frac{K_0 R}{E_a} \right] \quad (2)$$

From the Kissinger plot (Figure 10a), activation energy (E_a) and frequency factor were estimated. The reaction rate and Avrami exponent were also calculated from the equations. The evaluated kinetic parameter values are given in Table 1. The value of activation energy, which is required to break the bonds between the molecules, was found to be 69.1518 kJ/mol from the slope of the Ozawa plot (Figure 10b). The following equation, Equation (3), in which M_s is the starting mass, M_f is the final mass, and $M(t, T)$ is the instantaneous mass, which depends on temperature and time, describes the relationship between this parameter and the degree of conversion (Figure 11) of the compound with the same name.

$$\alpha = \frac{M_s - M(t, T)}{M_s - M_T} \quad (3)$$

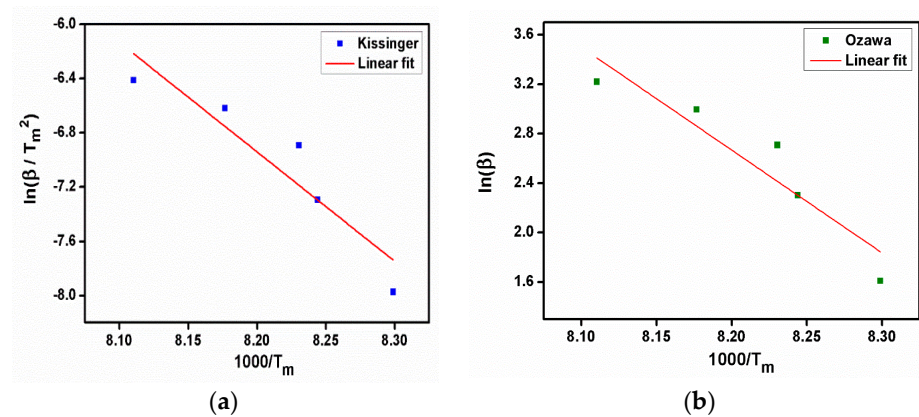


Figure 10. (a) Kissinger plot, (b) Ozawa plot of 2C5NA.

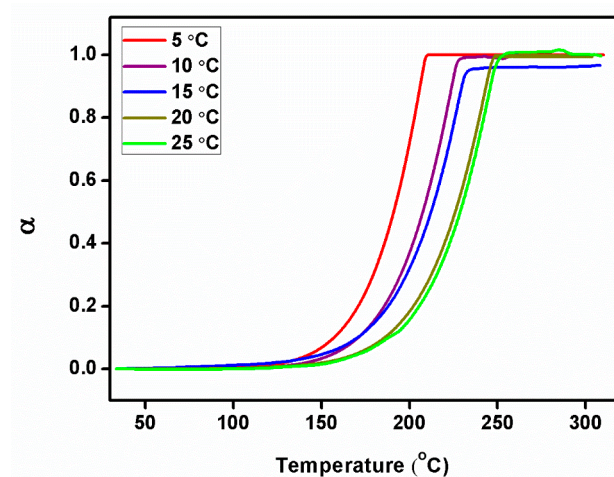


Figure 11. Degree of conversion plot of 2C5NA.

Table 1. Thermal kinetic parameters of 2C5NA.

(β) °C/min	T _m °C	E _a kJ/mol	K ₀ S ⁻¹	K S ⁻¹	R ²	n	α_{\max} min ⁻¹
5	120.5			4.4132		1.3593	0.03613
10	121.3			4.4138		0.9985	0.02552
15	121.5	67.1244	4.4158 × 10 ⁴	4.4140	0.8276	0.6901	0.02152
20	122.3			4.4149		0.7060	0.02121
25	123.3			4.4155		0.6213	0.01806

The kinetic models are useful to examine such constants available in an empirical relation of the Arrhenius equation. Hence, the real process of such materials can be identified under different thermal conditions as closely as possible. The calculation of kinetic parameters from the Kissinger and Ozawa methods is mainly dependent on the heating rate and peak temperature (i.e., melting point), so the methods present more reliable results on kinetic parameters.

Using the relation (Equation (3)), the degree of conversion (α) was estimated for various heating rates of the TG curves. The calculated α values can be applied to the Coats–Redfern and Friedman methods to estimate the values of E_a, the rate constant (K), frequency factor (K₀), and Avrami exponent (n) [21,22]. An estimated α_{\max} value is presented in Table 1.

3.5. Dielectric Analysis of 2C5NA

Dielectric analysis (DEA) of crystals is a technique used to study the electrical properties of crystalline materials as they respond to changes in temperature, frequency, or other environmental conditions. The analysis focuses on the dielectric constant, or permittivity, which is a measure of how a material responds to an applied electric field. DEA is particularly useful in investigating the polarization and dipole moments within crystals, as well as phase transitions and other dynamic processes. The dielectric analysis of an organic material can explore its applications in various fields. The dielectric behavior of any material depends on parameters like temperature, frequency of the electric field, chemical structure of the sample, grain boundaries, charge storage density, and charge transport capacity. The dielectric measurements were conducted for a title crystal with a size of 8.32 × 7.21 × 1.52 mm³ at various temperatures, such as 40, 60, 80, and 100 °C.

The plot (Figure 12a,b) represents the dielectric constant and dielectric loss as a function of log frequency at different temperatures of the 2C5NA crystal. The dielectric constant decreases when increasing the frequency up to 1 MHz. At low frequencies, a potential barrier is generated by the space charge polarization, which leads to a high value of the dielectric constant. This type of behavior is due to the space charge polarization effect. From the dielectric loss curve, the low value of dielectric loss observed at higher frequencies indicates the quality of the sample [23]. At low frequencies, the dielectric loss is moderately high, which is due to the high electrical resistivity of grains and their boundaries. Low dielectric loss is essential for the enhancement of nonlinear behavior [24]. Beyond 1 MHz, both dielectric constant and loss curves attained saturation. This variation can be due to the ionization process in the sample [25].

Figure 13a illustrates the frequency-dependent ac conductivity analysis at various temperatures. In the ac conductivity curve, there is no variation observed due to changing the temperature, other than at 40 °C, which reveals that the conduction process is not dependent on temperature in 2C5NA. The ac conductivity of the 2C5NA crystal was analyzed using the conductivity Equation (4). When the angular frequency is ω , the absolute permittivity in free space is ϵ_0 , and the phase degree is δ .

$$\sigma_{ac} = \epsilon_0 \epsilon_r \omega \tan \delta \quad (4)$$

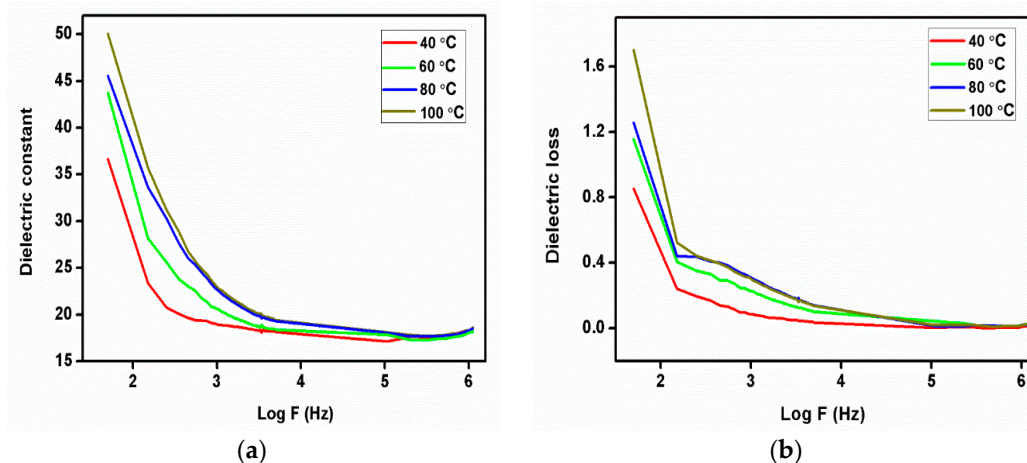


Figure 12. (a) Dielectric constant, (b) dielectric loss curve of 2C5NA.

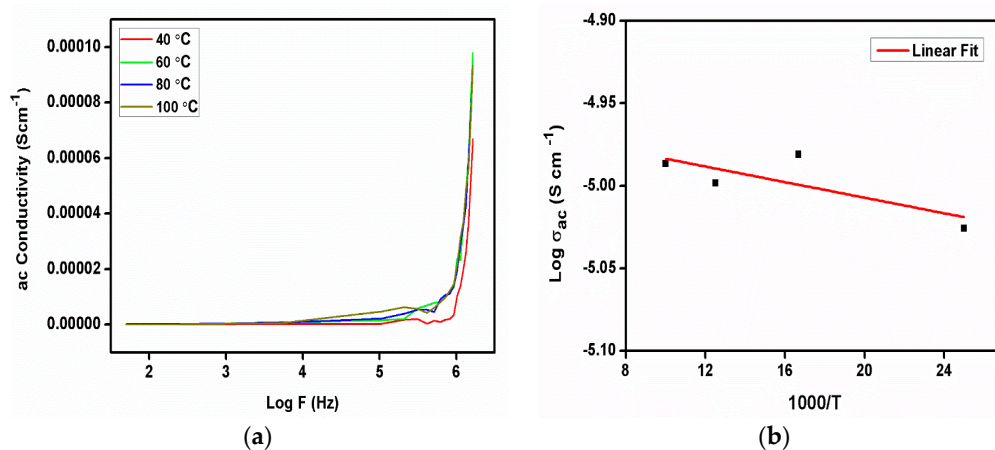


Figure 13. (a) ac conductivity curve, (b) Arrhenius plot of 2C5NA.

The value of ac conductivity was found to increase with frequency after 1 MHz. The dielectric polarization was created due to the formation of dipoles by activated localized charge carriers; hence, the dielectric relaxation process was found to increase beyond that frequency. The dielectric relaxation usually represents the formation of a reorientational process in solid materials. In the ac conductivity curve, it describes the interaction of the alternate current field with the motion of dipoles. The hopping conductivity mechanism can occur via tunneling or may be thermally activated. At high frequencies, slight variations in conductivity and the value of the activation energy indicate the blocking behavior of the grain boundaries present inside the crystal.

The activation energy for the charge jumping process was evaluated from the Arrhenius plot (Figure 13b). The value of the activation energy (E_a) was evaluated to be 0.204 eV for the title compound.

3.6. Vicker's Microhardness Test of 2C5NA

The Vickers microhardness test is a widely used method for measuring the hardness of materials, especially small or thin samples, with a high degree of precision. It is named after its inventor, George Vickers. The Vickers hardness test is based on the principle of indentation hardness, where a known force is applied to an indenter to create an impression on the material's surface. The size of the indentation is measured, and the hardness value is calculated from the indentation's dimensions. The Vickers microhardness analysis was performed on the grown sample. To reduce error, and maintain stability and reliability, the Vicker's hardness test was performed with standard materials and verified with their reports. The surface of the sample was cleaned and polished with wet, high-quality velvet

cloths. The dwell time was kept at 10 s for all loading. The indentation was started with the minimum applied load and we observed that the crystal was broken when applying the load of 25 g. Hence, the study was performed with loads less than 25 g. Hence, the test specimen or crystal can break due to many parameters such as weak intrinsic bonds, a higher number of grain boundaries (i.e., polycrystalline nature) on its surface, and poor load-withstanding capabilities. The value of the Vickers hardness number can be estimated by using the relation $H_V = 1.8544 P/d^2 \text{ kg mm}^{-2}$. The graph shows the variations between the applied load and the Vickers hardness number of the sample. The Mohs hardness number of the specimen was also evaluated using the equation $H_M = 0.675(H_V)^{1/3}$. The Vickers hardness number increases with the increasing applied load, which reveals the behavior of the reverse indentation size effect [26]. The graph represents the variation in the Vickers hardness number (Figure 14a) and Mohs hardness number (Figure 14b) with the function of load. The stiffness constant of the sample was estimated with the Wooster empirical relation $C_{11} = H_V^{7/4}$ and is displayed in Figure 14c.

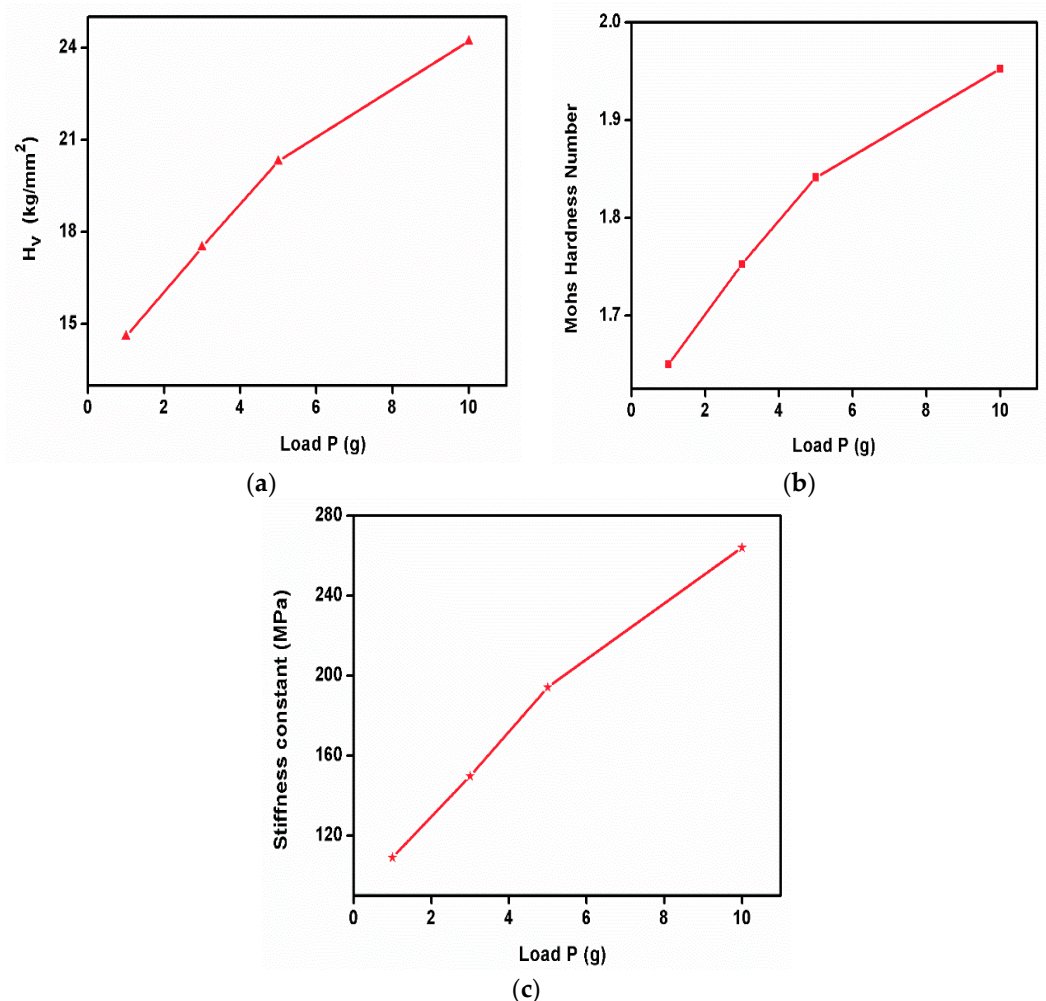


Figure 14. (a) Vicker's hardness number, (b) Mohs hardness number, (c) stiffness constant of 2C5NA.

4. Conclusions

A huge organic 2C5NA crystal was successfully produced in a single-wall ampoule utilizing the vertical Bridgman technique. The dimensions of the ampoule and cone angle were discussed in detail. A good-quality 2C5NA crystal was harvested from the ampoule with a cone angle of $13^\circ 40'$. The growth parameters were optimized, and the lowering rate of the ampoule with the 2C5NA compound was kept at 0.7–0.8 mm/hr. Hence, the homogenous melt was obtained and nucleation originated from the bottom of the cone. The crystal structure of the 2C5NA crystal was confirmed using single-crystal XRD and powder

XRD. The crystal belongs to a monoclinic crystal system with the space group P21/n. The lattice parameter values were obtained from single-crystal XRD and were well-matched with previously reported values. In addition to that, the proton NMR confirmed the structure of the grown crystal. Various types of vibrations, such as symmetric, asymmetric, stretching, in-plane, and out-plane, indicated the existence of functional groups in the 2C5NA crystal using FTIR. The thermal behavior of organic 2C5NA was analyzed with the TG-DTA curve, which revealed the melting and decomposition temperatures at 122 °C and 245 °C, respectively. The activation energy of 2C5NA was calculated to be 67.1244 and 69.1518 kJ/mol using the Kissinger and Ozawa equations, respectively. Other thermal kinetic parameters, such as rate constant (K), frequency factor (K_0), Avrami exponent (n), and degree of conversion (α_{\max}) values, were correlated with the TG-DTA curve. The dielectric response of the grown crystal was examined with respect to frequency at different temperatures. The activation energy was evaluated from the Arrhenius plot as 0.204 eV. The mechanisms of dielectric loss, ac conductivity, and relaxation processes were studied with corresponding curves. The mechanical behavior of grown crystals was thoroughly examined using Vickers microhardness studies, in which the grown 2C5NA crystal fits under the soft material category. From these findings, it would be a promising material for making non-linear optical and microelectronic devices.

Author Contributions: Conceptualization, methodology, software, validation, formal analysis, investigation, resources, data curation, project administration, funding acquisition, writing—original draft preparation, S.K. and K.D.B.; writing—review and editing, data curation, visualization, supervision, V.E.S. and P.S. All authors have read and agreed to the published version of the manuscript.

Funding: This research received no external funding.

Data Availability Statement: Data will be made available on reasonable request.

Acknowledgments: The authors gratefully acknowledge the crystal growth centre, Anna University, Chennai, for support and the utilization of facilities.

Conflicts of Interest: The authors declare no conflict of interest.

References

1. Szostak, M.M.; Chojnacki, H.; Saryga, E.; Dłużniewski, M.; Bąk, G.W. Contribution to molecular mechanism of optical nonlinearity and electric conductivity of 3-nitroaniline single crystals by dielectric, electric and quantum chemical studies. *Chem. Phys.* **2009**, *365*, 44–52. [[CrossRef](#)]
2. Yanishlieva, N.; Marinova, E.M. Effects of antioxidants on the stability of triacylglycerols and methyl esters of fatty acids of sunflower oil. *Food Chem.* **1995**, *54*, 377–382. [[CrossRef](#)]
3. Shaub, W.M. Procedure for estimating the heats of formation of aromatic compounds. Part II. Chlorinated phenols, biphenyls, diphenyl ethers and dibenzofurans. *Thermochim. Acta* **1983**, *62*, 315–323. [[CrossRef](#)]
4. Kanagasekaran, T.; Mythili, P.; Binay, K.; Gopalakrishnan, R. Effect of ion irradiation on the M-Nitroaniline single crystals. *Nucl. Instrum. Methods Phys. Res. B* **2010**, *268*, 36–41. [[CrossRef](#)]
5. Preeda, P.; Ganapathi Raman, R.; Sakthivel, P. Structural, FTIR, FT-Raman, optical and nonlinear optical properties of organic nonlinear optical crystal-3,5-diisopropyl-2-hydroxybenzoic acid. *Inorg. Chem. Commun.* **2022**, *146*, 110120. [[CrossRef](#)]
6. Corcoran, B.; Monat, C.; Grillet, C.; Moss, D.J.; Eggleton, B.J.; White, T.P.; Krauss, T.F. Green light emission in silicon through slow-light enhanced third-harmonic generation in photonic-crystal waveguides. *Nat. Photon.* **2009**, *3*, 206–210. [[CrossRef](#)]
7. Hernandez, C.F.; Ortiz, G.R.; Tseng, S.Y.; Gaj, M.P.; Kippelen, B. Third-harmonic generation and its applications in optical image processing. *J. Mater. Chem.* **2009**, *19*, 7394–7401. [[CrossRef](#)]
8. Silva, M.A.R.D.; Lima, L.M.S.S.; Amaral, L.M.; Ferreira, A.I.; Gomes, J.R. Standard molar enthalpies of formation, vapour pressures, and enthalpies of sublimation of 2-chloro-4-nitroaniline and 2-chloro-5-nitroaniline. *J. Chem. Thermodyn.* **2003**, *35*, 1343–1359. [[CrossRef](#)]
9. Saeed, A.; Ashraf, Z.; Batool, M.; Bolte, M. 2-Chloro-5-nitroaniline. *Acta Cryst.* **2009**, *65*, o1417. [[CrossRef](#)]
10. Medvediev, V.; Daszkiewicz, M. Structural and theoretical analysis of 2-chloro-4-nitroaniline and 2-methyl-6-nitroaniline salts. *Acta Cryst.* **2021**, *C77*, 125–136. [[CrossRef](#)]
11. Selvaraj, P.; Subramani, K.; Srinivasan, B.; Hsu, C.-J.; Huang, C.-Y. Electro-optical effects of organic N-benzyl-2-methyl-4-nitroaniline dispersion in nematic liquid crystals. *Sci. Rep.* **2020**, *10*, 14273. [[CrossRef](#)] [[PubMed](#)]

12. Liu, J.-B.; Li, Y.-X.; Zhang, X.-L.; Hua, X.-W.; Wu, C.-C.; Wei, W.; Wan, Y.-Y.; Cheng, D.-D.; Xiong, L.-X.; Yang, N.; et al. Novel Anthranilic Diamide Scaffolds Containing N-Substituted Phenylpyrazole as Potential Ryanodine Receptor Activators. *J. Agric. Food Chem.* **2016**, *64*, 3697–3704. [[CrossRef](#)] [[PubMed](#)]
13. Arjunan, V.; Marchewka, M.K.; Pietraszko, A.; Kalaivani, M. X-ray diffraction, vibrational and quantum chemical investigations of 2-methyl-4-nitroanilinium trichloroacetate trichloroacetic acid. *Spectrochim. Acta Part A Mol. Biomol. Spectrosc.* **2012**, *97*, 625–638. [[CrossRef](#)]
14. Hirose, M.; Okaniwa, M.; Miyazaki, T.; Imada, T.; Ohashi, T.; Tanaka, Y.; Arita, T.; Yabuki, M.; Kawamoto, T.; Tsutsumi, S.; et al. Design and synthesis of novel DFG-out RAF/vascular endothelial growth factor receptor 2 (VEGFR2) inhibitors: 3. Evaluation of 5-amino-linked thiazolo[5,4-d]pyrimidine and thiazolo[5,4-b]pyridine derivatives. *Bioorg. Med. Chem.* **2012**, *20*, 5600–5615. [[CrossRef](#)]
15. Volodymyr, V.; Medvediev, M.D. Intermolecular interactions in 2-methyl-3-nitroanilinium nitrate, sulphate and dihydrogen phosphate in a view of topological approach and vibrational spectra. *J. Mol. Struct.* **2021**, *1229*, 129577. [[CrossRef](#)]
16. Tabib, A.; Sdiri, N.; Elhouichet, H.; Férid, M. Investigations on electrical conductivity and dielectric properties of Na doped ZnO synthesized from sol gel method. *J. Alloys Compd.* **2015**, *622*, 687–694. [[CrossRef](#)]
17. Karuppusamy, S.; Dinesh Babu, K.; Sakthivel, P. Evaluation of thermal, dielectric and mechanical behavior of 4-nitrophenol crystal. *Chem. Phys. Lett.* **2022**, *807*, 140098. [[CrossRef](#)]
18. Karuppusamy, S.; Muralidharan, S.; Dinesh Babu, K.; Sakthivel, P. Thermal, dielectric, mechanical and structural behavior of 2-amino 4-methylpyridinium 4-nitrophenolate 4-nitrophenol bulk single crystal. *Heliyon* **2023**, *9*, E18260. [[CrossRef](#)]
19. Barbara, H.S. *Infrared Spectroscopy: Fundamentals and Applications*; John Wiley & Sons, Inc.: Hoboken, NJ, USA, 2004. [[CrossRef](#)]
20. Suresh, N.; Selvapandiyam, M.; Sakthivel, P.; Loganathan, K. Structural, Optical, Thermal, and Magnetic properties of strontium nitrate doped L-Alanine crystal. *Optik* **2020**, *221*, 165336. [[CrossRef](#)]
21. Coats, A.W.; Redfern, J.P. Kinetic parameters from Thermogravimetric data. II. *Polym. Lett.* **1965**, *3*, 917–920. [[CrossRef](#)]
22. Henry, L.F. Kinetics of Thermal Degradation of Char-Forming Plastics from Thermogravimetry. Application to a Phenolic Plastic. *J. Polym. Sci. Part C Polym. Symp.* **1964**, *6*, 183–195. [[CrossRef](#)]
23. Justin Raj, C.; Dinakaran, S.; Krishnan, S.; Milton Boaz, B.; Robert, R.; Jerome Das, S. Studies on optical, mechanical and transport properties of NLO active l-alanine formate single crystal grown by modified Sankaranarayanan–Ramasamy (SR) method. *Opt. Commun.* **2008**, *281*, 2285–2290. [[CrossRef](#)]
24. Deshmukh, K.; Basheer Ahamed, M.; Deshmukh, R.R.; Khadheer Pasha, S.K.; Bhagat, P.R.; Chidambaram, K. 3-Biopolymer Composites With High Dielectric Performance: Interface Engineering. *Biopolym. Compos. Electron.* **2017**, *27*–128. [[CrossRef](#)]
25. Haque, M.M.; Huq, M.; Hakim, M.A. Densification, magnetic and dielectric behaviour of Cu-substituted Mg–Zn ferrites. *Mater. Chem. Phys.* **2008**, *112*, 580–586. [[CrossRef](#)]
26. Obeid, A.; Roumie, M.; Badawi, M.S.; Awad, R. Evaluation of the Effect of Different Nano-Size of WO₃ on the Structural and Mechanical Properties of HDPE. *J. Inorg. Organomet. Polym.* **2022**, *32*, 1506–1519. [[CrossRef](#)]

Disclaimer/Publisher’s Note: The statements, opinions and data contained in all publications are solely those of the individual author(s) and contributor(s) and not of MDPI and/or the editor(s). MDPI and/or the editor(s) disclaim responsibility for any injury to people or property resulting from any ideas, methods, instructions or products referred to in the content.